https://doi.org/10.5194/egusphere-2025-3096
Preprint. Discussion started: 10 July 2025


# Crustal-upper mantle velocity structure from the North Qilian to Beishan block and the tectonic significance of the crustal deformation

Xiaosong Xiong [1*], Yingkang Li[2], Xuanhua Chen[1], Guowei Wu[1], Rui Gao[3], Jennifer D. Eccles[4]

[1] Chinese Academy of Geological Sciences, Beijing, 10009, China
[2] Geological Cores and Samples of Natural Resources, CGS, Sanhe, 065201, China
[3] School of Earth Science and Geological Engineering, Sun Yat-sen University, Guangzhou 510275, China
[4] School of Environment, University of Auckland, Auckland 1142, New Zealand

* Corresponding author: Xiaosong Xiong (benxung@126.com)

**Abstract** The Qilian Shan constitutes a Cenozoic fold-thrust belt characterized by multi-stage tectonic deformation since the Paleozoic. The Hexi corridor basins and the Beishan block, located north of the Qilian Shan, are the southern segment of the Central Asian Orogenic Belt. The crustal-mantle structure of the study area serves as a transition zone, crucial for comprehending the deep processes of accretion and crustal deformation. This study introduces a newly acquired 460-km seismic wide angle and refraction profile spanning the North Qilian Shan to the Beishan block. The P-wave velocity structure of the crust and upper mantle indicates a crustal thickness between 47.5 km and 60 km, segmented into five strata. The central Jiuquan basin displays the most substantial crust, measuring 59.5–60 km in thickness. The average crustal velocity varies between 6.24 and 6.43 km/s, while the Pn velocity ranges from 7.7 km/s to 8.1 km/s. The considerable variance in crustal velocity indicates heterogeneity in the crustal composition of the Qilian Shan and Beishan block. The southern edge fault of the Beishan block delineates the area, where northward and southward thrusting induces upper crustal deformation on opposing sides. The crust of the southern Beishan block is weaker than that of the bordering regions. Additionally, we propose a north-direction subduction polarity of the Qilian Ocean based on the northward-tilted velocity contour in Paleozoic.

**Keywords:** North Qilian; Beishan Block; Crustal-upper mantle velocity structure; crustal deformation

The Qilian Shan exhibits a Cenozoic fold-thrust belt with multi-stage tectonic deformation since Paleozoic. North of the Qilian Shan, the Hexi corridor basins and the Beishan block form the southern section of the Central Asian Orogenic Belt. Acting as a transition zone, the crustal-mantle structure of the studied area is crucial for comprehending the region including the Qilian Shan and Beishan block operates as the contact zone between the northeastern Tibetan plateau (NE Tibet) and the southern CAOB. This region acts as the transition zone between the Tethys tectonic domain and the Paleo-Asian oceanic (PAO) tectonic domain since the Paleozoic (Fig. 1a; Li et al. 1982; Yin and Harrison 2000; Xiao et al. 2009; Zhao et al. 2018). The NW-SE-trending Qilian Shan, situated in NE Tibet, is bordered by the Altyn Tagh fault to the west, the northern Qaidam thrust system to the south, the Haiyuan fault to the east, and the north Qilian Shan fault to the north (Figure 1b). The present-day Qilian Shan has witnessed Cenozoic reactivation as a fold-thrust belt (Zuza et al. 2017, 2019), enduring multi-stage tectonic deformation prior to the Cenozoic (Yin and Harrison 2000; Gehrels et al. 2003; Song et al. 2014; Wu et al. 2016; Zuza et al. 2017). The Beishan block, sometimes referred to as the Beishan orogenic belt (Liu 1995; Yuan et al. 2015; He et al. 2018; Li et al. 2023), is inside the middle of the South Tienshan-Beishan-Solonker suture zone (Fig. 1b). Experiencing multi-stage breakup, subduction, collision, and amalgamation during the closure of the PAO, mainly in the Paleozoic (Fig. 1; Zuo et al. 1991; Yue and Liou 1999; Wang et al. 2010; Xiao et al. 2010; Zuo and Li 2011; Şengör 2015), the geological history of the Beishan block is further complicated by regional extension overlap, subsequent intracontinental overthrusting, and strike-slip faulting since Mesozoic (Zheng et al. 1996; Xiao et al. 2010; Zuo and Li 2011; Zhang and Cunningham 2012; Li et al. 2023). The NE-trending grabens in the Gobi Altai, southeastern Mongolia and Beishan forms a rift system, associated with the termination of the final subduction

https://doi.org/10.5194/egusphere-2025-3096
Preprint. Discussion started: 10 July 2025


of the PAO (Meng 2003; Donskaya et al. 2008; Cunningham et al. 2009; Davis and Darby 2010) or the Cenozoic Indian-Eurasian collision (Zhang et al. 2007, 2021; Buslov 2012). This study proposes a new-acquired 460-km-long seismic wide angle and refraction profile encompassing the North Qilian Shan-to- Beishan block. The crustal-upper mantle P-wave velocity structure reveals the crustal thickness ranging from 47.5 to 60 km, divided into five layers. The central Jiuquan basin has the thickest crust at 59.5–60 km. Average crustal velocity ranges from 6.24 to 6.43 km/s, and Pn velocity of 7.7–8.1 km/s. Notably, the considerable variance in crustal velocity shows inhomogeneity non the crustal composition of the Qilian Shan and Beishan block. Bounded by the southern edge fault of the Beishan block, north-direction and south-direction thrusting contribute to upper crustal deformation to separate sides. The crust of the southern Beishan block is weaker than that of the bordering regions. Additionally, we propose a north-direction subduction polarity of the Qilian Ocean based on the northward-tilted velocity contour in Paleozoic.

In Cenozoic, the far-field effect of the Indian-Eurasian collision led to the outward expansion of NE Tibet, spreading across the Hexi corridor basins into the Beishan block or the Mongolian Altai Mountains (Mts.) (Cunningham 2013; Zheng et al. 2017; Wang et al. 2022). The reactivated Qilian Shan finally became an important part of the Tibet plateau, playing a significant role in researching the intracontinental convergence, thrusting-folding and the northern extension of NE Tibet (Meyer et al. 1998; Yuan et al. 2013; Zuza et al. 2017). As the southernmost CAOB, the Beishan block also served as a major place for examining the reactivation of the ancient crust and the transmission of compressional stress arising from the outward exhumation of NE Tibet and the Mongolian plateau in Cenozoic.

While previous geophysical studies have been conducted in the Qilian Shan– Beishan block transition zone to comprehend the subduction polarity, continental extension, foundering and magmatic activities (Xiao et al. 2012; HUANG et al. 2014; Wei et al. 2017; Xu et al. 2019; Shen et al. 2020; Huang et al. 2021; Yang et al. 2024), the crustal-upper mantle structure remains ambiguous due to limited resolution quality. In this study, a N-S-trending 460-km-long seismic wide angle and refraction profile sweeps throughout the North Qilian, Hexi corridor (containing the Jiuquan basin and the Huahai basin), and the entire Beishan block was done. This profile reflects the high-quality crustal-upper mantle velocity structure of the research area. Combined with other geological and geophysical datasets, we examined the tectonic consequence of the key characteristics of the velocity structure, hoping to throw light on the northern extension of the NE Tibet plateau, and the reactivation of the Beishan crust.

## Geological setting

The Beishan block is positioned between the Mongolia collage system in the north and the Dunhuang Block in the south (Fig. 1; Zuo et al. 1991; Yue and Liou 1999; Wang et al. 2010; Xiao et al. 2010; Zuo and Li 2011). It is widely considered to encompass multiple different terranes, including the Que'ershan, Hanshan, Mazongshan, Shuangyingshan, and Shibanshan terranes. They are separated by four nearly parallel W-E-trending ophiolite mélange zones, named Hongshishan-Baiheshan (F1), Shibanjing-Xiaohuangshan (F2), Hongliuhe-Xichangjing (F3) and Liuyuan-Huitongshan-Zhangfangshan (F4) respectively (Fig. 1c; Zuo et al. 1991; Liu 1995; Wei et al. 2004; Ao et al. 2010, 2012, 2016; Xiao et al. 2010; Yang et al. 2010; Zuo and Li 2011; He et al. 2014; Wang et al. 2017; Wei et al. 2017; He et al. 2018; Wang et al. 2018; Li et al. 2022; Li et al. 2023). The Hongliuhe-Xichangjing suture zone (F3) is generally recognized as the final sealing position of the South Beishan Block and North Beishan block in middle-late Ordovician (Li et al. 2022). The Hexi corridor, sandwiched between the Beishan block and the Qilian Shan by the southern margin fault of the Beishan (F5) and northern margin fault of the North Qilian (F8), is a Cenozoic foreland basin system (Fig. 1b; Li et al. 2002). The basement of the Hexi corridor consists predominantly Paleozoic rocks, covered by thick Mesozoic and Cenozoic deposits. In this study region, The Hexi corridor is divided into the Huahai basin in the north and Jiuquan basin in the south by the Kuantanshan-Heishan fault (F6). The Huahai basin is part of the Dunhuang block, traditionally assigned as a Precambrian cratonic block or a microcontinent (BGMRGP 1989; Che and Sun 1996; Mei et al. 1997; Mei 1998; Yu et al. 1998; Ren et al. 1999; Xu et al. 1999; Lu et al. 2008; Liu et al. 2009; Zhang et al. 2011; He et al. 2013; Zong et al. 2013), and involved in the final collision of the PAO (Shi et al. 2022). The Jiuquan basin, a subbasin of the Hexi Corridor foreland

https://doi.org/10.5194/egusphere-2025-3096
Preprint. Discussion started: 10 July 2025


basin, has deposited Cenozoic sediments since as early as ca. 40 Ma (Dai et al. 2005; Wang et al. 2016), and was subsequently influenced by the uplift of the North Qilian since Cenozoic. The early Paleozoic Qilian Shan, recording the closure of the Qilian Ocean as part of the Proto-Tethys Ocean (Yu et al. 2021), is a classic orogen traditionally divided into three structural units: the North Qilian Shan Orogenic belt (NQS), the Central Qilian block, and the South Qilian thrust belt (Yin and Harrison 2000). The previous two units are delimited by the North Qilian fault (F9). The NQS principally comprises early Paleozoic ophiolite suites (Fig. 1c), blueschists, eclogites, greenschists, and arc-related magmatic and volcanic rocks (Xu et al. 2005; Zhang et al. 2007; Song et al. 2009; Xiao et al. 2009; Zhao et al. 2024). These strata are overlain by Silurian flysch, Devonian molasse and Carboniferous-Triassic sedimentary periods (Wang et al. 2023). In Mesozoic, the extensional and transtensional basins evolved over the Qilian Shan from the Xining Basin in the south to the Hexi corridor in the north (Horton et al. 2004; Pan et al. 2004). In Cenozoic, the Qilian Shan has been reactivated as a fold-thrust belt to accommodate the crustal deformation resultant from the Indian-Eurasian collision with development of massive thrusts and strike-slip faults (Tapponnier et al. 1990; Zuza et al. 2019).

## Data and methods

### seismic collection and processing

In 2018, The Chinese Academy of Geological Sciences completed a SW-NE-trending seismic wide-angle reflection and refraction profile stretching from the North Qilian to the Beishan block. Nine TNT blasts, ranging from 1.5 to 3.0 tons, were exploded throughout the seismic profile at intervals of roughly 30–60 km (ZB0–ZB8, shown in red stars in Fig. 1c). To achieve thorough coverage, 250 portable seismographs (depicted as blue circles in Fig. 1c) were strategically distributed along the whole seismic profile at a spacing of 2–3 km. This deployment sought to capture high-quality seismic data, and the specific parameters of the shots are presented in Table 1.

### Identification of Seismic phases

To make the seismic records clearer, each trace was bandpass filtered up to 8 Hz and displayed in reduced time based on a velocity of 6 km/s in the breadth of -5–10 s (e.g. Fig. 2, Fig. 3). Six seismic phases, including Pg, P1, P2, P3, P4, Pm and Pn, are identified based on the reduced seismic recordings (Fig. 2, Fig. 3). Pg is a first arriving phase propagating over the crystalline basement. Pm is the strongly wide-angle reflected phase from the Moho discontinuity. Pn is the head wave refracted phase from the top of the mantle with a characteristic velocity of 7.7–8.0 km/s. P2–P4 are the reflected phases from the intracrustal second-order velocity interfaces. In Fig. 2 and Fig. 3, the dotted lines represent the identified phases, and the squares mark the position of the computed traveltime.

The first-arrivals of Pg are picked up to offset of 100 km. the travetime of ZB1 is early, which reveals the shallow velocity of the NQS is high with 5.1–6.3 km/s and 4.0–6.1 km/s average velocity correspondingly. The traveltime of the north branch of ZB8 is early too, demonstrating the shallow crustal velocity in the northern Beishan block is with 3.3–6.3 km/s. Intracrustal reflection phases P2–P4 can be recognized at the offset ranges from 70–90 km, 100–150 km, and 120–150 km respectively. Pm can be corelated over an offset of 180 km for most shots (Fig. 4a). Pn was found with maximal amplitude in the offset range of 240–280 km (Fig. 3). The Pn displayed in shot ZB1 seismic record is with 7.9–8.1 km/s velocity, while 7–8.1 km in shot ZB8 (Fig. 4).

## The velocity structure model

The 2-D crustal velocity structure is based on seismic phases identification, and the first 2-D crustal model is built with the greatest elevation 4300 m as the datum. The forward fitting calculation adopts the asymptotic ray tracing to fit the traveltime of each shot (Fig. 4 (Cerveny et al. 1988; Vidale 1988; Zelt and Smith 1992; Cervený 2001) and gradually improves the initial 2-D velocity structure by constantly modifying the interface depth and interval velocity. The travetime fitting of 5–6 phases for nine shots are conducted step by step to limit the multi-solution of the model. Fig. 4 illustrates the traveltime fitting of the seismic recordings of the shot gather and the

https://doi.org/10.5194/egusphere-2025-3096
Preprint. Discussion started: 10 July 2025


complete crustal ray coverage. The time error of the ray tracing forward fitting accuracy is typically less than 0.05 s, and the maximum is not more than 0.1 s. The root mean square error (RMS) of the traveltime fitting for different earthquake phases is reported in Table 2. The velocity inaccuracy is controlled within 0.05 km/s, while the Moho depth error is less than 1 km. The ultimate crustal-upper mantle velocity structure is found in Fig. 5. The result shows the crust can be split into upper crust (from the surface to P2), middle crust (from P2 to P3), and lower crust (from P3 to the Moho discontinuity). The upper crust can be separated into two layers by intracrustal interface C1 determined by seismic phase P2. The lower crust can be separated into two strata as well as intracrustal interface C4 indicated by seismic phase P4.

## Velocity structure of the upper crust

The upper crust, comprising the layer from the surface to interface C2, has pronounced lateral segmentation. Notably, a lower velocity zone is prevalent in the North Qilian-Jiuquan basin, contrasting with a significantly greater velocity zone in the Beishan block. Along interface C1 amid the upper crust, many high-velocity entities with an interval velocity of 6.3–6.4 km/s are seen.

The base of interface C1 corresponds to the basement surface, characterized by a velocity range of 3.4–6.5 km/s. The basement profile undulates extensively within the depth of 6.1–12.5 km (Fig. 5b). The interval velocity measures 5.2–6.05 km/s, with an interface depth of 6.3–7.2 km in the middle Qilian. In the southern North Qilian, the interval velocity ranges from 5.2–6.1 km/s, having a high-velocity body in the bottom section with an interval velocity of 6.2–6.45 km/s, and the interface depth lowers to 10.8–11.4 km. In the northern section of the North Qilian, the interval velocity falls to 4.0–6.0 km/s, while the interface depth deepens to 9.7–10.1 km. In the Jiuquan basin, the interval velocity reduces to 3.6–6.1 km/s, with an interface depth falling to 11.2–12.5 km. The Huahai basin has an interval velocity of 3.8–6.2 km/s, and the interface depth ranges from 11.5–12.5 km. Additionally, a high-velocity body with an interval velocity of 6.3–6.5 km/s appears at the bottom below the F5 fracture. In the southern Beishan block, layer velocities on the south side measure 4.6–6.2 km/s, with interface depths ranging from 11.5–12.0 km, whereas on the north side, layer velocities reduce to 3.4–6.1 km/s, and interface depths are 9.4–11.3 km. In the Northern Beishan block, layer velocities are 4.2–6.2 km/s, with an interface depth of 10.5–12.5 km. Further north in the Beishan block, the interval velocity is 4.2–6.2 km/s, and the interface depth is 10.0–11.3 km. At the bottom of the Beishan block, multiple high-velocity bodies are observed with layer velocities of 6.3–6.4 km/s, including the high-velocity body under the Mazhoushan terrane. The bottom layer exhibits velocities ranging from 6.0–6.3 km/s and interface depths ranging from 13.2–27.6 km. While lacking significant lateral segmentation, this layer exhibits considerable interface undulations (Fig. 5b). South of fault F9, the interval velocity is 6.05–6.15 km/s, with an interface depth of 12.8–18.3 km. Between faults F9 and F5, the layer thickens substantially, and the interface depth climbs to 17.6–27.5 km. North of fault F5, the layer thickness reduces to match the southernmost part of the profile, but the velocity increases to 6.1–6.4 km/s. This characteristic shows that the North Qilian and the Jiuquan basin have a consistent basement, matching with the residual gravity anomaly findings (Yang et al. 2024).

**velocity structure of the middle crust**

The zoning features of the intermediate crust are notably different from the top crust, with interface depth of 23.4–38.7 km, and layer velocities of 6.2–6.5 km/s. There're comparatively low-velocity zones occurring in the northern North Qilian and Jiuquan basins (Fig. 5b). The depth of the contact between the NQS and the Jiuquan basin is 23.4–38.7 kilometers. The minimum interval velocity is 6.2–6.35 km/s in the middle Qilian, increasing to 6.25–6.45 km/s northward. The interface depth in the Huahai basin is 27.5–38.7 km, with interval velocity 6.25–6.5 km/s, and the maximum interval velocity reaches 6.32–6.45 km/s in the middle region (Fig. 5b). The interface depth in the Beishan block decreases to 24.4–31.2 km. The interval velocity in the Shibanshan arc is 6.3–6.5 km/s, whereas those in the southern Shuangyingshan terrane decrease to 6.25–6.4 km/s. The interval velocity increases to 6.3–6.42 km/s. Velocity contours in the Qilian and the Jiuquan basin show an undulating northward inclination pattern, while those in the Huahai basin dip steeply to the south (Fig. 5b).

https://doi.org/10.5194/egusphere-2025-3096
Preprint. Discussion started: 10 July 2025


**velocity structure of the lower crust**

The lower crust can be typically separated into three portions from south to north bordered by F9 and F4 (Fig. 5b). The undulation of the interface C4 and Moho discontinuity is consistent, which signifies the thickness of the upper and lower layers of the lower crust is with the same trend along the complete profile.

Upper layer: in this layer, with a bottom depth of 36.7–49.5 km and interval velocity of 6.45–6.7 km/s (Fig. 5b), distinguishing features emerge. South of fault F9, interface C4 is located at a depth of 36.7–42.4 km, indicating an interval velocity of 6.45–6.7 km/s. Between faults F9 and F4, interface C4 deepens to 38.6–49.2 km, and the interval velocity increases to 6.5–6.7 km/s. Notably, a substantial upward undulation of a high-velocity body is found in this zone. North of F4, interface C4 is positioned at a depth of 37.4–40.3 km, and the interval velocity decreases to 6.47–6.65 km/s.

Lower layer: The Moho discontinuity is identified at a depth of 47.5–60 km, and the lower layer exhibits an interval velocity of 6.65–6.85 km/s (Fig. 5b). In the Qilian Shan and Jiuquan basin, the Moho is at a depth of 57.8–60 km, with an interval velocity of 6.7–6.85 km/s. The central part of the Jiuquan basin displays the deepest Moho at 60 km, accompanied by a decrease in interval velocity to 6.7–6.78 km/s. In the Huahai basin and Beishan block, the Moho depth spans from 47.5–57 km, and the velocity of the layer reduces to 6.7–6.75 km/s. The shallowest Moho, at 47.5 km, is recorded in the Que'ershan terrane, with an interval velocity of 6.65–6.78 km/s.

**Pn velocity structure**

The Pn velocity structure exhibits nuances throughout the analyzed locations. The Qilian Shan shows a top-of-the-upper-mantle velocity range of 7.9–8.4 km/s, with approximately flat contours. From the Jiuquan basin to the Shibanshan terrane, the velocity reduces to 7.7–8.3 km/s, then rises to 7.9–8.6 km/s in the Shuangyingshan terrane. The Mazongshan, Hanshan, and Que'ershan terranes have decreasing Pn velocities of 7.8–8.5 km/s, indicating a progressive drop from south to north. The lowest Pn velocity (7.7–7.8 km/s) is reported beneath faults F5, F1, and F6.

**Crustal Velocity Structure Implications**

The crustal velocity structure proposes an unusual scenario where the deepest Moho is found in the central Jiuquan basin, rather than the North Qilian Shan with the highest elevation. Additionally, the Qilian Shan and southern Shibanshan terrane exhibit a thin upper-middle crust and a thick lower crust, while other parts have the reverse pattern (Fig. 5b)

## Crustal-upper mantle velocity anomaly structure

To improve the sensitivity of the velocity heterogeneity of the crustal-upper mantle structure, the contour of the velocity anomaly structure of the crustal-upper mantle is determined (Fig. 6b, the difference between the velocity contour values and their mean values). Figure 6b demonstrates that in the upper layer of the crust from depths of 0 to 12.5 km, the composition is significantly inhomogeneous, and lateral segmentation is visible. The Qilian Shan is with a high positive velocity anomaly (0.3–1.0 km/s). The Jiuquan basin and Huahai basin are with negative velocity anomaly (-1.1–-0.15 km/s), and extend northward to the southern Shuangyingshan terrane, which are prevented by the strong positive velocity anomaly in the central Shuangyingshan terrane. Three positive velocity anomaly bodies (0.12–0.45 km/s) with closed contour exist beneath the faults F5, F4, and the core Shuangyingshan terrane. In the northern Shuangyingshan terrane, a negative velocity anomaly (-1.3–-0.12 km/s) develops, and thins out to the north extending to the southern Mazongshan terrane. The positive velocity anomaly (0.15–0.45 km/s) starting from the Mazongshan terrane dives northward to the northern end of the Que'ershan terrane, and the central part is covered by the low-velocity negative anomalies (-0.4–-0.08 km/s) in the upper Hanshan terrane.

At a depth of 9.2–38.5 km between interface C1and C3, the middle Qilian and the southern North Qilian consisted of the northward-tilted, small-variation positive velocity anomalies (0.0 to 0.08 km/s) and negative anomalies (-0.03–-0.01 km/s). The northern North Qilian, the Jiuquan basin and the southern portion of the Huahai basin are northward-tilted, downward-curved layers of the

https://doi.org/10.5194/egusphere-2025-3096
Preprint. Discussion started: 10 July 2025


low-velocity negative anomalies (-0.05–-0.2 km/s). The northern half of the Huahai basin and the Shibanshan terrane are positive anomaly (0.0–0.08 km/s) layers with small velocity changes. The southern Shuangyingshan terrane is a mixed layer of the positive velocity anomaly (0.01–0.08 km/s) and negative velocity anomaly (-0.01–-0.04 km/s). The velocity anomaly from the northern Shuangyingshan terrane to the Que'ershan terrane is positive (0.03–0.12 km/s), and only locally negative (-0.01–-0.03 km/s).

In the upper layer of the lower crust, the Qilian Shan is characterized by a positive velocity anomaly (0.01-0.12 km/s) in the upper section, and a negative velocity anomaly (-0.01-0.08 km/s) in the lower part. The Jiuquan basin and Huahai basin are characterized by minor negative velocity anomalies (-0.02–-0.08 km/s). The Beishan block is characterized by a strong positive velocity anomaly (0.02-0.12 km/s) and exhibits a northward-increasing trend (Fig. 6b). In the lowest layer of the lower curst, From the North Qilian to the southern Huahai basin, the velocity anomaly reveals positive (0.01-0.07 km/s) with a relatively minor variance. From the northern Huahai basin to the southern Shuangyingshan terrane, the velocity anomaly is with a positive to negative (0.01–-0.07 km/s) from top to bottom. From the northern Shuangyingshan to the Que'ershan terrane, lesser positive anomalies (0.01 to 0.03 km/s) are observed (Fig. 6b).

At the top of the upper mantle, the North Qilian Shan and the southern Jiuquan basin show positive velocity anomaly with modest changes (0.05-0.15 km/s), whereas negative anomaly with substantial velocity variations (-0.1 to -0.25 km/s) from the northern Jiuquan basin to the Shibanshan terrane. The southern Shuangyingshan terrane is characterized with a gradient of the velocity anomaly ranging from negative to positive (-0.1–0.12 km/s). The northern Shuangyingshan and Mazongshan display positive anomaly (0.03–0.12 km/s) moving downwardly. The southern Hanshan terrane has a positive anomaly (0.01–0.1) characterized by a gradual reduction from south to north. The northern Hanshan terrane and the Que'ershan terrane show negative anomaly (-0.01–-0.12) that diminish steadily from south to north (Fig. 6b).

## Discussion

The observed crustal-upper mantle structure (Fig. 5; Fig. 6) is a complicated outcome shaped by both vertical and lateral material transport processes. These activities are related to Paleozoic subduction, collision, and accretion events, Mesozoic intracontinental deformations, and the Cenozoic northward spread of the NE Tibetan since the Precambrian.

### Subduction polarity of the Qilian Ocean and the southern PAO

The North Qilian Ocean, a part of the Proto-Tethys Ocean, evolved predominantly along the Kunlun Mts., Qilian Shan and Altyn Mts. in the northern Tibetan Plateau. The closure of the Qilian Ocean resulting from the collision between the Kunlun-Qaidam continent and the southern boundary of the North China Craton remains a matter of considerable debate (Yin and Harrison 2000; Guterch et al. 2003; Xiao et al. 2009; Song et al. 2014; Wu et al. 2017; Zuza et al. 2017). The subduction polarity of this ocean has been proposed as: 1) north-dipping (Zuo and Liu 1987; Song et al. 2013; Li et al. 2022); 2) south-dipping (Wang and Liu 1981; Li et al. 2016); 3) bidirectional (Zhao et al. 2024); or divergent (Wu et al. 2011; Chen et al. 2019). While past geophysical investigations have covered the Qilian Shan (Xiao et al. 2016; Guo et al. 2019; Shen et al. 2020; Li et al. 2021), concentration has largely been on neotectonics rather than Paleozoic evolution.

Our data demonstrates a northward-tilted velocity contour from interface C2 to the topmost mantle beneath the Qilian Shan (Fig. 5b). This inclination suggests the northward descent of the middle crust to the uppermost mantle beneath the Hexi corridor. We speculate that this trait reflects a north-dipping subduction polarity of the Qilian Ocean in the early Paleozoic. Further corroborating our thought is the negative velocity anomaly body spanning from the lower crust to the topmost mantle beneath the Hexi corridor and southern Shibanshan (Fig. 6b).

The Central Asian Orogenic Belt (CAOB) is well acknowledged for its southward migration throughout development and composition from 1000 Ma to 250 Ma (Lehmann and al. 2010; Jian et al. 2014; Kröner et al. 2014; Xiao et al. 2018). Consequently, the Dunhuang block, positioned at the southernmost extent of the CAOB and associated with the Beishan block, assumes a vital role in unraveling the decisive closure of the southern Paleo-Asian Ocean (PAO). Despite detailed geochemical and chronological research on Paleozoic rocks in the Dunhuang block and the Beishan block, the amalgamation style of the PAO remains elusive (Xiao et al. 2010; Shi et al. 2020, 2021;

https://doi.org/10.5194/egusphere-2025-3096
Preprint. Discussion started: 10 July 2025


Li et al. 2023).

The previous Golmud–Ejin seismic profile defined the crustal structure of the Beishan block into three strata with an active upper mantle and stable crust (Cui et al. 1995), consistent with our current profile. The stable crust, specifically the middle-lower crust, is crucial in conserving fossil architecture. The north-tilted velocity contour beneath the Que'ershan terrane from interface C2 to the Moho discontinuity implies the crust north of the Que'ershan subducted beneath the Hanshan terrane, a deduction supported by geological observations (Xiao et al. 2018; Duan et al. 2020; Niu et al. 2020; Xin et al. 2020). Consequently, we suggest the subduction polarity of the Hongshishan Ocean as south-direction. The zone between F9 and F1 faults reveals a peculiar undulation of velocity profiles, presumably caused by subsequent late Paleozoic collision or bidirectional compression in the Cenozoic, complicating the distinction of subduction direction. Combining geological findings (Yu et al. 2012; Hu et al. 2015; Song et al. 2015; Wang et al. 2015), we propose that the positive velocity anomaly body in the upper mantle between faults F2 and F4 could represent the fossil breakoff subduction slab following the north-dipping subduction of the Beishan Ocean, marked by the Hongliuhe–Xichangjing ophiolite mélange (Li et al. 2023).

**Crustal deformation mechanism**

Situated between the Tibetan Plateau and Mongolian plateau, the crust from the Qilian Shan to the Beishan block has undergone intracontinental deformation to varied degrees (Cunningham 2010, 2013; Zhang et al. 2023). The Qilian Shan, regarded as the youngest uplifted Mts. of the Tibetan plateau, absorbs significant shortening strain (Gaudemer et al. 1995; Meyer et al. 1998; Gao et al. 2013; Zuza et al. 2017), by a series of parallel NW-SE-trending thrust faults (Meyer et al. 1998; Tapponnier et al. 2001; Yuan et al. 2013; Zuza et al. 2017). Progressive deformation commenced in Miocene, extending northward to the Hexi corridor and Beishan–Alxa block (Wang et al. 2020; Yu et al. 2021; Zhang et al. 2023). The seismic profiles (Fig. 5b, Fig. 6b) reveal two distinct downward-undulation velocity contours on either side of the southern boundary fault of the Beishan (F5). This suggests F5 as the boundary fault restricting compressional stress from the north and south.

In the area south of F5, northward-tilted positive velocity anomaly bodies with 6.2–6.45 km/s velocity at the base of the upper crust form the Qilian Shan to the Shibanshan terrane, correlate to the north-direction thrust faults. In the area north of F5, the opposite velocity features imply north-direction thrusting in the upper crust of the Beishan block. The downward-undulation of the velocity contours imply co-thickening of the middle-lower curst of the NQS–Shuangyingshan area, with the upper crust experiencing thrusting and overthrusting. Our velocity structure indicated that low Pn velocity with 7.7–7.9 km/s and dome-shaped uplift of the crust directly beneath F5 (Fig. 5b). The electrical resistivity imaging also highlighted the boundary fault, termed Baihewan fault (BHWF in Fig. 7) in the southernmost Shibanshan terrane, which penetrates the lower crust with low resistivity, to both sides of which the direction of the thrusting is opposing (Yang et al. 2019). The shallow velocity structure across the Huahai basin and the southern Beishan block likewise depicted the differences to both sides of F5(Wu et al. 2022), which is aligned with our result (Wu et al. 2022). Collectively, we suggest F5 is a large-scale strike-slip fault which restricts the stress transmission further to both sides. The projected left slip rate with 1.52–2.69 mm/a, is substantially greater than the thrust rate with 0.35 mm/a in the southernmost Beishan area (Yang et al. 2019; Yun et al. 2021). The GPS motion and velocity rate result reveals the moving direction changed from northeast in the Qilian Shan to nearly-east in the Beishan block with a significant lateral motion rate (Fig. 7). These results further lend support to our result. Thus, the crustal deformation in this transition zone is different in the areas to both sides of F5. In the area south of F5, the upper and middle-lower crust is decoupled, and the deformation mechanism in the upper crust in north-direction thrusting, and co-thickened in the middle-lower crust (Fig. 8). The Seismic reflection profile revealed a south-dipping Cenozoic thrusting system that dislocated the Paleozoic–Mesozoic strata over the undeformed Meso-Cenozoic sediments in the Jiuquan basin (Zuza et al. 2016; Huang et al. 2021), which is compatible with our seismic imaging. Guo et al. (2019) also found the deformation and expansion of the Qilian Shan extended across the Hexi corridor by overthrusting in the top crust and thickening in the lower crust east to our study area. The seismic reflection profile over the southern segment of this section further supports the thickening mechanism of the middle-lower crust by duplexing (Huang et al. 2021). In the southern Beishan block north of F5, the north-direction thrust faults was playing the function in the top crust, and the middle-lower crust is folded alike the North

https://doi.org/10.5194/egusphere-2025-3096
Preprint. Discussion started: 10 July 2025


Qilian–Hexi corridor area.

In NE Tibet and Beishan area, earthquakes predominantly occur in the Qilian Shan, Hexi Corridor basins, Huahai Basin, and local areas west of Liyuan, Hongliuhe, and Xingxingxia area, mostly at depths of 15–16 km (Fig. 7). The Beishan area is very stable, with few known earthquakes higher than magnitude 4.7 (Xiong et al. 2003; Yang et al. 2019; Zhao et al. 2019). The current low topographic relief also shows the Beishan block is relatively stable and tectonically inactive. However, our imaging suggests a slight bending of the middle-lower crust in the southern Beishan block, suggesting the middle-lower crust of the southern Beishan block is a little weaker than the bordering regions. Active left-lateral and thrust faults in the southern Beishan block support this assumption (Yang et al. 2019; Zhang et al. 2020; Yun et al. 2021; Zhang et al. 2023).

## Conclusion

The crust thickness in the studied area spans from 47.5 to 60 km, separated into five strata. The thickest crust, measuring 58–60 km, spans from the Qilian Shan to the middle Jiuquan basin and gradually thins northward, with thicknesses of 55–58 km in the Dunhuang block, 51.5–55 km in the Shibanshan arc, and 47.5–51.5 km in the Shuangyingshan and Que'ershan terranes. Surprisingly, the deepest Moho (60 km deep) is found in the middle Jiuquan basin, not in the North Qilian Shan with the highest height. The average crustal velocity varies from 6.24 to 6.43 km/s, with crustal velocity fluctuations between 3.4 and 6.85 km/s. The velocity at the top of the upper mantle is observed at 7.7–8.1 km/s.

The study region is grouped into three parts based on present-day activity: the Qilian-Hexi corridor, the southern Beishan block, and the northern Beishan. The middle unit has softer crust compared to the others, and the deformation of the middle-lower crust in the southern Beishan block is considerably stronger than in the other two units.

(3) Subduction in the research area involves both north-direction and south-direction subduction of the Qilian Ocean and the Hongshishan Ocean.

(4) Bounded by F5 operating as a regional large-scale strike-slip fault, the crustal deformation process on both sides is similarly disconnected. In the Qilian-Hexi corridor, north-direction thrusting and overthrusting dominate, while in the Beishan block, south-direction thrusting and overthrusting rule. The middle-lower crust co-thickens throughout the entire research area.

**Acknowledgments** This work was jointly funded by the National natural Science Foundation of the China (Grant Nos. 42274134, 41774114, 42261144669), the China Geological Survey Project (Grant No. DD20230008, DD20179342 and DD20160083) and the China Scholarship Council.

## References

Ao, S., Xiao, W. *et al.* 2016. Paleozoic accretionary orogenesis in the eastern Beishan orogen: Constraints from zircon U–Pb and 40Ar/39Ar geochronology. *Gondwana Research*, **30**, 224-235, https://doi.org/https://doi.org/10.1016/j.gr.2015.03.004

Ao, S.J., Xiao, W.J., Han, C.M., Mao, Q.G. and Zhang, J.E. 2010. Geochronology and geochemistry of Early Permian mafic–ultramafic complexes in the Beishan area, Xinjiang, NW China: Implications for late Paleozoic tectonic evolution of the southern Altaids. *Gondwana Research*, **18**, 466-478, https://doi.org/https://doi.org/10.1016/j.gr.2010.01.004

Ao, S.J., Guo, Q.Q. *et al.* 2012. Cambrian to early Silurian ophiolite and accretionary processes in the Beishan collage, NW China: implications for the architecture of the Southern Altaids. *Geological Magazine*, **149**, 606-625, https://doi.org/10.1017/S0016756811000884

BGMRGP. 1989. Regional Geology of Gansu Province. Geological Publishing House Beijing, China [in Chinese with English abstract].

Buslov, M.M. 2012. Geodynamic nature of the Baikal Rift Zone and its sedimentary filling in the Cretaceous–Cenozoic: the effect of the far-range impact of the Mongolo-Okhotsk and Indo-Eurasian collisions. *Russian Geology and Geophysics*, **53**, 955-962, https://doi.org/https://doi.org/10.1016/j.rgg.2012.07.010

Cerveny, P.F., Naeser, N.D., Zeitler, P.K., Naeser, C.W. and Johnson, N.M. 1988. History of Uplift and Relief of the Himalaya During the Past 18 Million Years: Evidence from Fission-Track Ages of Detrital Zircons from Sandstones of the Siwalik Group. *In*: Kleinspehn, K.L. and Paola, C. (eds) *New Perspectives in Basin Analysis*. Springer New York, New York, NY, 43-61, https://doi.org/10.1007/978-

https://doi.org/10.5194/egusphere-2025-3096
Preprint. Discussion started: 10 July 2025


1-4612-3788-4_3

Cervený, V. 2001. *Seismic ray theory*. Cambridge university press Cambridge [in Chinese with English abstract].

Che, Z.C. and Sun, Y. 1996. The age of the Altun granulite facies complex and the basement of the Tarim basin. *Regional Geology of China*, **56**, 51-57 [in Chinese with English abstract].

Chen, X., Gao, R., Xiong, X., Shao, Z., Li, B. and Zhang, Y. 2019. Deep seismic reflection profiling and broad-band magnetotelluric sounding of the Qilian Orogenic Belt: evidence for bi-directional subduction of the Proto-Tethys Ocean plate and northward growth of the Qinghai-Tibet Plateau. *AGU Fall Meeting Abstracts*, T22C-03 [in Chinese with English abstract].

Cui, Z.-z., Li, Q.-s., Wu, C.-d., Yin, Z.-x. and Liu, H.-b. 1995. The crustal and deep structures in Golmud-Ejin Qi GGT. *Acta Geophysica Sinica*, **38**, 28-34 [in Chinese with English abstract].

Cunningham, D. 2010. Tectonic setting and structural evolution of the Late Cenozoic Gobi Altai orogen. *Geological Society, London, Special Publications*, **338**, 361-387, https://doi.org/https://doi.org/10.1144/SP338.17

Cunningham, D. 2013. Mountain building processes in intracontinental oblique deformation belts: Lessons from the Gobi Corridor, Central Asia. *Journal of Structural Geology*, **46**, 255-282, https://doi.org/https://doi.org/10.1016/j.jsg.2012.08.010

Cunningham, D., Davies, S. and McLean, D. 2009. Exhumation of a Cretaceous rift complex within a Late Cenozoic restraining bend, southern Mongolia: implications for the crustal evolution of the Gobi Altai region. *Journal of the Geological Society*, **166**, 321-333, https://doi.org/10.1144/0016-76492008-082

Dai, S., Fang, X., Chunhui, S., Junping, G., Donglin, G. and Jijun, L. 2005. Early tectonic uplift of the northern Tibetan Plateau. *Chinese Science Bulletin*, **50**, 1642-1652, https://doi.org/10.1360/03wd0255

Davis, G.A. and Darby, B.J. 2010. Early Cretaceous overprinting of the Mesozoic Daqing Shan fold-and-thrust belt by the Hohhot metamorphic core complex, Inner Mongolia, China. *Geoscience Frontiers*, **1**, 1-20, https://doi.org/https://doi.org/10.1016/j.gsf.2010.08.001

Donskaya, T.V., Windley, B.F. *et al.* 2008. Age and evolution of late Mesozoic metamorphic core complexes in southern Siberia and northern Mongolia. *Journal of the Geological Society*, **165**, 405-421, https://doi.org/10.1144/0016-76492006-162

Duan, L., Niu, W. *et al.* 2020. The petrogenesis of quartz diorite(350 Ma)from the Baiheshan area of the Beishan orogenic belt, and its chronological constraint on Hongshishan-Baiheshan Ocean's subduction initiation. *Geological Bulletin of China*, **39**, 1330-1340 [in Chinese with English abstract].

Gao, R., Hou, H. *et al.* 2013. Fine crustal structure beneath the junction of the southwest Tian Shan and Tarim Basin, NW China. *Lithosphere*, **5**, 382-392 [in Chinese with English abstract].

Gaudemer, Y., Tapponnier, P. *et al.* 1995. Partitioning of crustal slip between linked, active faults in the eastern Qilian Shan, and evidence for a major seismic gap, the 'Tianzhu gap', on the western Haiyuan Fault, Gansu (China). *Geophysical Journal International*, **120**, 599-645, https://doi.org/10.1111/j.1365-246X.1995.tb01842.x

Gehrels, G.E., Yin, A. and Wang, X.-F. 2003. Detrital-zircon geochronology of the northeastern Tibetan plateau. *GSA Bulletin*, **115**, 881-896, https://doi.org/10.1130/0016-7606(2003)115<0881:DGOTNT>2.0.CO;2

Guo, G., Wu, C. *et al.* 2019. Seismic anisotropy of the northeastern margin of the Tibetan Plateau derived from analysis of SKS and Pms seismic phases. *Chinese Journal of Geophysics*, **62**, 1650-1662 [in Chinese with English abstract].

Guterch, A., Grad, M., pi ák, A., Brückl, E., Hegedüs, E., Keller, G.R. and Thybo, H. 2003. Special Contribution: An Overview of Recent Seismic Refraction Experiments in Central Europe. *Studia geophysica et geodaetica*, **47**, 651-657, https://doi.org/10.1023/A:1024775921231

He, Z.-Y., Zhang, Z.-M., Zong, K.-Q. and Dong, X. 2013. Paleoproterozoic crustal evolution of the Tarim Craton: Constrained by zircon U–Pb and Hf isotopes of meta-igneous rocks from Korla and Dunhuang. *Journal of Asian Earth Sciences*, **78**, 54-70, https://doi.org/https://doi.org/10.1016/j.jseaes.2013.07.022

He, Z.-Y., Klemd, R., Yan, L.-L. and Zhang, Z.-M. 2018. The origin and crustal evolution of microcontinents in the Beishan orogen of the southern Central Asian Orogenic Belt. *Earth-Science Reviews*, **185**, 1-14, https://doi.org/https://doi.org/10.1016/j.earscirev.2018.05.012

He, Z., Zong, K., Jiang, H., Xiang, H. and Zhang, Z. 2014. Early Paleozoic tectonic evolution of the southern Beishan orogenic collage: Insights from the granitoids. *Acta Petrologica Sinica*, **30**, 2324-2338, [in Chinese with English abstract].

Horton, B.K., Dupont-Nivet, G., Zhou, J., Waanders, G.L., Butler, R.F. and Wang, J. 2004. Mesozoic-Cenozoic evolution of the Xining-Minhe and Dangchang basins, northeastern Tibetan Plateau:

https://doi.org/10.5194/egusphere-2025-3096
Preprint. Discussion started: 10 July 2025


Magnetostratigraphic and biostratigraphic results. *Journal of Geophysical Research: Solid Earth*, **109**, https://doi.org/https://doi.org/10.1029/2003JB002913

Hu, P.-y., Zhai, Q.-g., Jahn, B.-m., Wang, J., Li, C., Lee, H.-y. and Tang, S.-h. 2015. Early Ordovician granites from the South Qiangtang terrane, northern Tibet: Implications for the early Paleozoic tectonic evolution along the Gondwanan proto-Tethyan margin. *Lithos*, **220-223**, 318-338, https://doi.org/https://doi.org/10.1016/j.lithos.2014.12.020

Huang, X., Gao, R., Li, W. and Xiong, X. 2021. Seismic reflection evidence of crustal duplexing and lithospheric underthrusting beneath the western Qilian Mountains, northeastern margin of the Tibetan Plateau. *Science China Earth Sciences*, **64**, 96-109, https://doi.org/10.1007/s11430-020-9677-y

HUANG, Z.-X., LI, H.-Y. and XU, Y. 2014. Lithospheric S-wave velocity structure of west China and neighboring areas from surface wave tomography. *Chinese Journal of Geophysics*, **57**, 3994-4004 [in Chinese with English abstract].

Jian, P., Kröner, A. *et al.* 2014. Zircon dating of Neoproterozoic and Cambrian ophiolites in West Mongolia and implications for the timing of orogenic processes in the central part of the Central Asian Orogenic Belt. *Earth-Science Reviews*, **133**, 62-93, https://doi.org/https://doi.org/10.1016/j.earscirev.2014.02.006

Kröner, A., Kovach, V. *et al.* 2014. Reassessment of continental growth during the accretionary history of the Central Asian Orogenic Belt. *Gondwana Research*, **25**, 103-125, https://doi.org/https://doi.org/10.1016/j.gr.2012.12.023

Lehmann, J., Schulmann, K. *et al.* 2010. Structural constraints on the evolution of the Central Asian Orogenic Belt in SW Mongolia. *American Journal of Science*, **310**, 575-628, https://doi.org/https://doi.org/10.2475/07.2010.02

Li, B., Qi, B. *et al.* 2023. Two-phase kinematic evolution of the Qilian Shan, northern Tibetan Plateau: Initial Eocene−Oligocene deformation that accelerated in the mid-Miocene. *Geological Society of America Bulletin*, https://doi.org/10.1130/B37159.1

Li, B., Zuza, A.V. *et al.* 2021. Corrigendum to Cenozoic multi-phase deformation in the Qilian Shan and out-of-sequence development of the northern Tibetan Plateau [Tectonophysics 782–783 (2020) 228423]. *Tectonophysics*, **808**, 228794, https://doi.org/https://doi.org/10.1016/j.tecto.2021.228794

Li, C., Wang, Q., Liu, X. and Tang, Y. 1982. *Explanatory notes to the tectonic map of Asia*. Geological Publishing House, Beijing [in Chinese with English abstract].

Li, G.-J., Wang, Q.-F., Huang, Y.-H., Gao, L. and Yu, L. 2016. Petrogenesis of middle Ordovician peraluminous granites in the Baoshan block: Implications for the early Paleozoic tectonic evolution along East Gondwana. *Lithos*, **245**, 76-92, https://doi.org/https://doi.org/10.1016/j.lithos.2015.10.012

Li, J., Wu, C. *et al.* 2022. Tectonic setting of metamorphism and exhumation of eclogite-facies rocks in the South Beishan orogen, northwestern China. *Geosphere*, **19**, 100-138, https://doi.org/10.1130/GES02548.1

Li, S., Huang, F. and Li, H. 2002. Post-collisional lithosphere delamination of the Dabie-Sulu orogen. *Chinese Science Bulletin*, **47**, 259-263, https://doi.org/10.1360/02tb9063

Liu, X. 1995. Tectonics of orogenic belts in Beishan Mts., western China and their evolution. *Dixue Yanjiu (Geosci. Research)*, **28**, 37-48 [in Chinese with English abstract].

Liu, Y., Yu, H., Xin, H., Lu, S., Xiu, Q. and Li, Q. 2009. Tectonic units division and Precambrian significant geological events in Altyn Tagh Mountain, China. *Geological Bulletin of China*, **28**, 1430-1438 [in Chinese with English abstract].

Lu, S., Li, H., Zhang, C. and Niu, G. 2008. Geological and geochronological evidence for the Precambrian evolution of the Tarim Craton and surrounding continental fragments. *Precambrian Research*, **160**, 94-107, https://doi.org/https://doi.org/10.1016/j.precamres.2007.04.025

Mei, H. 1998. Archean tonalite in the Dunhuang, Gansu Province: Age from the U-Pb single zircon and Nd isotope. *Process Precamb. Research*, **21**, 41-45 [in Chinese with English abstract].

Mei, H., Yu, H., Li, Q. and Zuo, G. 1997. Preliminary litho-tectonic framework of early Precambrian rocks in Dunhuang-Beishan area, Gansu, west China. *Progress in Precambrian Research*, **20**, 47-54, [in Chinese with English abstract].

Meng, Q.-R. 2003. What drove late Mesozoic extension of the northern China–Mongolia tract? *Tectonophysics*, **369**, 155-174, https://doi.org/https://doi.org/10.1016/S0040-1951(03)00195-1

Meyer, B., Tapponnier, P. *et al.* 1998. Crustal thickening in Gansu-Qinghai, lithospheric mantle subduction, and oblique, strike-slip controlled growth of the Tibet plateau. *Geophysical Journal International*, **135**, 1-47, https://doi.org/10.1046/j.1365-246X.1998.00567.x

Niu, W., Xin, H., Duan, L., Zhao, Z., Zhang, G., Ren, B. and Zhang, Y. 2020. Geochemical characteristics, zircon U-Pb age of SSZ ophiolite in the Baiheshan area of the Beishan orogenic belt, Inner Mongolia, and its indication for the evolution of the Paleo-Asian Ocean. *Geological Bulletin of China*, **39**, 1317-1329 [in Chinese with English abstract].

https://doi.org/10.5194/egusphere-2025-3096
Preprint. Discussion started: 10 July 2025


Pan, G.-t., Zhu, D.-c. and Wang, L.-q. 2004. Bangong Lake-Nu River suture zone-the northern boundary of Gondwanaland: Evidence from geology and geophysics. *Earth Science Frontiers*, **11**, 371-382 [in Chinese with English abstract].

Ren, J., Wang, Z. *et al.* 1999. The Tectonics of China from a Global View A Guide to the Tectonic Map of China and Adjacent Regions. *Beijing: Geol. Publ. House* [in Chinese with English abstract].

Şengör, A. 2015. The Founder of Modern Geology Died 100 Years Ago:: The Scientific Work and Legacy of Eduard Suess. *Geoscience Canada*, **42**, 181-246 [in Chinese with English abstract].

Shen, X., Li, Y. *et al.* 2020. Lateral growth of NE Tibetan Plateau restricted by the Asian lithosphere: Results from a dense seismic profile. *Gondwana Research*, **87**, 238-247, https://doi.org/https://doi.org/10.1016/j.gr.2020.06.018

Shi, M., Hou, Q., Wu, C., Yan, Q., Cheng, N., Zhang, Q.W.L. and Wang, H.Y.C. 2021. Origins of the meta-mafic rocks in the southern Dunhuang Block (NW China): Implication for tectonic framework of the southernmost Central Asian Orogenic Belt. *Geological Journal*, **56**, 3959-3973, https://doi.org/https://doi.org/10.1002/gj.4144

Shi, M., Hou, Q. *et al.* 2020. Paleozoic Sanweishan arc in the northern Dunhuang region, NW China: The Dunhuang block is a Phanerozoic orogen, not a Precambrian block. *Journal of Asian Earth Sciences*, **194**, 103954, https://doi.org/https://doi.org/10.1016/j.jseaes.2019.103954

Shi, Z., Gao, R., Lu, Z., Li, W., Li, H., Huang, X. and Liang, H. 2022. Bidirectional subduction of the Bangong-Nujiang ocean revealed by deep-crustal seismic reflection profile. *Tectonophysics*, **837**, 229455, https://doi.org/https://doi.org/10.1016/j.tecto.2022.229455

Song, D., Niu, G., Zhang, C. and Zhang, G. 2009. Time constraints on orogenesis from oceanic subduction to continental subduction, collision, and exhumation: An example from North Qilian and North Qaidam HP-UHP belts. *Acta Petrologica Sinica*, **25**, 2067-2077 [in Chinese with English abstract].

Song, D., Xiao, W., Han, C. and Tian, Z. 2014. Polyphase deformation of a Paleozoic forearc–arc complex in the Beishan orogen, NW China. *Tectonophysics*, **632**, 224-243, https://doi.org/https://doi.org/10.1016/j.tecto.2014.06.030

Song, D., Xiao, W., Windley, B.F., Han, C. and Tian, Z. 2015. A Paleozoic Japan-type subduction-accretion system in the Beishan orogenic collage, southern Central Asian Orogenic Belt. *Lithos*, **224-225**, 195-213, https://doi.org/https://doi.org/10.1016/j.lithos.2015.03.005

Song, S., Niu, Y., Su, L. and Xia, X. 2013. Tectonics of the North Qilian orogen, NW China. *Gondwana Research*, **23**, 1378-1401, https://doi.org/https://doi.org/10.1016/j.gr.2012.02.004

Tapponnier, P., Zhiqin, X., Roger, F., Meyer, B., Arnaud, N., Wittlinger, G. and Jingsui, Y. 2001. Oblique Stepwise Rise and Growth of the Tibet Plateau. *Science*, **294**, 1671-1677, https://doi.org/10.1126/science.105978

Tapponnier, P., Meyer, B. *et al.* 1990. Active thrusting and folding in the Qilian Shan, and decoupling between upper crust and mantle in northeastern Tibet. *Earth and Planetary Science Letters*, **97**, 382-403, https://doi.org/https://doi.org/10.1016/0012-821X(90)90053-Z

Vidale, J. 1988. Finite-difference calculation of travel times. *Bulletin of the Seismological Society of America*, **78**, 2062-2076, https://doi.org/10.1785/BSSA0780062062

Wang, C.-Y., Lou, H., Silver, P.G., Zhu, L. and Chang, L. 2010. Crustal structure variation along 30° in the eastern Tibetan Plateau and its tectonic implications. *Earth and Planetary Science Letters*, **289**, 367-376, [in Chinese with English abstract].

Wang, C., Deng, J., Lu, Y., Bagas, L., Kemp, A.I.S. and McCuaig, T.C. 2015. Age, nature, and origin of Ordovician Zhibenshan granite from the Baoshan terrane in the Sanjiang region and its significance for understanding Proto-Tethys evolution. *International Geology Review*, **57**, 1922-1939, https://doi.org/10.1080/00206814.2015.1043358

Wang, D., Luo, L., Tang, Y., Yin, F., Wang, B., Wang, L. and Center, C. 2016. Zircon U-Pb dating and petrogenesis of Early Paleozoic adakites from the Niujingshan ophiolitic mélange in the Changning-Menglian suture zone and its geological implications. *Acta Petrologica Sinica*, **32**, 2317-2329 [in Chinese with English abstract].

Wang, H.Y.C., Wang, J. *et al.* 2017. Metamorphic evolution and geochronology of the Dunhuang orogenic belt in the Hongliuxia area, northwestern China. *Journal of Asian Earth Sciences*, **135**, 51-69, https://doi.org/https://doi.org/10.1016/j.jseaes.2016.12.014

Wang, Q. and Liu, X. 1981. Qilian Mountains Caledonian Polycyclic Double Metamorphic Belt. *Collection of papers on the geotectonics of China and its neighboring regions Beijing: Geological Publishing House*, 92-101 [in Chinese with English abstract].

Wang, S., Zhang, K., Song, B., Li, S., Li, M. and Zhou, J. 2018. Geochronology and geochemistry of the Niujuanzi ophiolitic mélange, Gansu Province, NW China: implications for tectonic evolution of the Beishan Orogenic Collage. *International Journal of Earth Sciences*, **107**, 269-289, https://doi.org/10.1007/s00531-017-1489-2

https://doi.org/10.5194/egusphere-2025-3096
Preprint. Discussion started: 10 July 2025


Wang, T., Huang, H. *et al.* 2022. Voluminous continental growth of the Altaids and its control on metallogeny. *National Science Review*, **10**, https://doi.org/10.1093/nsr/nwac283

Wang, W., Zheng, D. *et al.* 2020. Cenozoic Exhumation of the Qilian Shan in the Northeastern Tibetan Plateau: Evidence From Low‐Temperature Thermochronology. *Tectonics*, **39** [in Chinese with English abstract].

Wang, Z., Xiong, X., Wu, G., Li, Z., Ye, Z. and Jin, Z. 2023. Crustal structure and deformation mechanism of the western northeast Tibetan Plateau. *Frontiers in Earth Science*, **11**, https://doi.org/10.3389/feart.2023.1255813

Wei, X., Jiang, M., Liang, X., Chen, L. and Ai, Y. 2017. Limited southward underthrusting of the Asian lithosphere and material extrusion beneath the northeastern margin of Tibet, inferred from teleseismic Rayleigh wave tomography. *Journal of Geophysical Research: Solid Earth*, **122**, 7172-7189, https://doi.org/https://doi.org/10.1002/2016JB013832

Wei, Z., Huang, Z., Jin, X., Sun, Y. and Huo, J. 2004. Geological characteristics of ophiolite migmatitic complex of Hongshishan region, Gansu. *Northwest Geol*, **37**, 13-18 [in Chinese with English abstract].

Wu, C., Yin, A., Zuza, A.V., Zhang, J., Liu, W. and Ding, L. 2016. Pre-Cenozoic geologic history of the central and northern Tibetan Plateau and the role of Wilson cycles in constructing the Tethyan orogenic system. *Lithosphere*, **8**, 254-292, https://doi.org/10.1130/L494.1

Wu, C., Gao, Y. *et al.* 2011. An early Palaeozoic double-subduction model for the North Qilian oceanic plate: evidence from zircon SHRIMP dating of granites. *International Geology Review*, **53**, 157-181, https://doi.org/10.1080/00206810902965346

Wu, C., Zuza, A.V. *et al.* 2017. Geochronology and geochemistry of Neoproterozoic granitoids in the central Qilian Shan of northern Tibet: Reconstructing the amalgamation processes and tectonic history of Asia. *Lithosphere*, **9**, 609-636, https://doi.org/10.1130/L640.1

Wu, G., Xiong, X. *et al.* 2022. 2D Tomographic imaging of the P-wave velocity structure in the upper crust beneath the southern Beishan tectonic belt. *Earth Science Frontiers*, **29**, 402-415, https://doi.org/10.13745/j.esf.sf.2022.2.2

Xiao, Q., Zhang, J., Wang, J., Zhao, G. and Tang, J. 2012. Electrical resistivity structures between the Northern Qilian Mountains and Beishan Block, NW China, and tectonic implications. *Physics of the Earth and Planetary Interiors*, **200-201**, 92-104, https://doi.org/https://doi.org/10.1016/j.pepi.2012.04.008

Xiao, Q., Shao, G., Yu, G., Cai, J. and Wang, J. 2016. Electrical resistivity structures of the Kunlun–Qaidam–Qilian system at the northern Tibet and their tectonic implications. *Physics of the Earth and Planetary Interiors*, **255**, 1-17, https://doi.org/https://doi.org/10.1016/j.pepi.2016.03.011

Xiao, Q., Yu, G., Liu-Zeng, J., Oskin, M.E. and Shao, G. 2017. Structure and geometry of the Aksay restraining double bend along the Altyn Tagh Fault, northern Tibet, imaged using magnetotelluric method. *Geophysical Research Letters*, **44**, 4090-4097, https://doi.org/https://doi.org/10.1002/2017GL072581

Xiao, W., Windley, B.F., Yong, Y., Yan, Z., Yuan, C., Liu, C. and Li, J. 2009. Early Paleozoic to Devonian multiple-accretionary model for the Qilian Shan, NW China. *Journal of Asian Earth Sciences*, **35**, 323-333, https://doi.org/https://doi.org/10.1016/j.jseaes.2008.10.001

Xiao, W., Windley, B.F. *et al.* 2018. Late Paleozoic to early Triassic multiple roll-back and oroclinal bending of the Mongolia collage in Central Asia. *Earth-Science Reviews*, **186**, 94-128, https://doi.org/https://doi.org/10.1016/j.earscirev.2017.09.020

Xiao, W., Qigui, M. *et al.* 2010. Paleozoic multiple accretionary and collisional processes of the Beishan orogenic collage. *American Journal of Science*, **310**, 1553-1594, https://doi.org/10.2475/10.2010.12]

Xin, H., Niu, W., Tian, J., Teng, X. and Duan, X. 2020. Spatio-temporal structure of Beishan orogenic belt and evolution of Paleo-Asian Ocean, Inner Mongolia. *Geological Bulletin of China*, **39**, 1297-1316 [in Chinese with English abstract].

Xiong, Z.-Q., Qian, W., Suzuki, K. and O. McNamara, J. 2003. Formation of Complement Membrane Attack Complex in Mammalian Cerebral Cortex Evokes Seizures and Neurodegeneration. *The Journal of Neuroscience*, **23**, 955, https://doi.org/10.1523/JNEUROSCI.23-03-00955.2003

Xu, Q., Pei, S., Yuan, X., Zhao, J., Liu, H., Tu, H. and Chen, S. 2019. Seismic Evidence for Lateral Asthenospheric Flow Beneath the Northeastern Tibetan Plateau Derived From S Receiver Functions. *Geochemistry, Geophysics, Geosystems*, **20**, 883-894, https://doi.org/https://doi.org/10.1029/2018GC007986

Xu, X.-Y., Xia, L.-Q. and Xia, Z.-C. 2005. Volcanism and mineralization in the North Qilian Orogenic Belt, Northwestern China. Springer Berlin Heidelberg, Berlin, Heidelberg, 487-489. https://doi.org/10.1007/3-540-27946-6_126

Xu, Z., Yang, J., Zhang, J., Jiang, M., Li, H. and Cui, J. 1999. A comparison between the tectonic

https://doi.org/10.5194/egusphere-2025-3096
Preprint. Discussion started: 10 July 2025


units on the two sides of the Altun sinistral strike-slip fault and the mechanism of lithospheric shearing. *Acta Geologica Sinica*, **73**, 193-205 [in Chinese with English abstract].

Yang, H., Xiong, S., Liu, Q., Zhou, D., Yang, X., Fan, Z. and Jia, Z. 2024. Tectonic framework of Qilian orogen: reveal from an aeromagnetic anomaly feature. *Applied Geophysics*, https://doi.org/10.1007/s11770-023-1041-z

Yang, H., Li, Y. *et al.* 2010. Character and structural attribute of the Beishan ophiolite. *Northwestern Geology*, **43**, 26-36 [in Chinese with English abstract].

Yang, H., Yang, X. *et al.* 2019. Quaternary Activity of the Beihewan Fault in the Southeastern Beishan Wrench Belt, Western China: Implications for Crustal Stability and Intraplate Earthquake Hazards North of Tibet. *Journal of Geophysical Research: Solid Earth*, **124**, 13286-13309, https://doi.org/https://doi.org/10.1029/2018JB017209

Yin, A. and Harrison, T.M. 2000. Geologic Evolution of the Himalayan-Tibetan Orogen. *Annual Review of Earth and Planetary Sciences*, **28**, 211-280, https://doi.org/doi:10.1146/annurev.earth.28.1.211

Yu, H., Mei, H. and Li, Q. 1998. The characteristics of Archean khondalite series in Dunhuang, Gansu Province. *Progress in Precambrian Research*, **21**, 19-25 [in Chinese with English abstract].

Yu, J., Li, X., Wang, G., Wu, P. and Yan, Q. 2012. Zircon U-Pb ages of Huitongshan and Zhangfangshan ophiolite in Beishan of Gansu-Inner Mongolia border area and their significance. *Geological Bulletin of China*, **31**, 2038-2045 [in Chinese with English abstract].

Yu, S., Peng, Y. *et al.* 2021. Tectono-thermal evolution of the Qilian orogenic system: Tracing the subduction, accretion and closure of the Proto-Tethys Ocean. *Earth-Science Reviews*, **215**, 103547, https://doi.org/https://doi.org/10.1016/j.earscirev.2021.103547

Yuan, D.-Y., Ge, W.-P. *et al.* 2013. The growth of northeastern Tibet and its relevance to large-scale continental geodynamics: A review of recent studies. *Tectonics*, **32**, 1358-1370, https://doi.org/https://doi.org/10.1002/tect.20081

Yuan, Y., Zong, K. *et al.* 2015. Geochemical and geochronological evidence for a former early Neoproterozoic microcontinent in the South Beishan Orogenic Belt, southernmost Central Asian Orogenic Belt. *Precambrian Research*, **266**, 409-424, https://doi.org/https://doi.org/10.1016/j.precamres.2015.05.034

Yue, Y. and Liou, J.G. 1999. Two-stage evolution model for the Altyn Tagh fault, China. *Geology*, **27**, 227-230, https://doi.org/10.1130/0091-7613(1999)027<0227:TSEMFT>2.3.CO;2

Yun, L., Zhang, J. *et al.* 2021. Discovery of active faults in the southern Beishan area, NW China: implications for regional tectonics. *Journal of Geomechanics*, **27**, 195-207 [in Chinese with English abstract].

Zelt, C.A. and Smith, R.B. 1992. Seismic traveltime inversion for 2-D crustal velocity structure. *Geophysical Journal International*, **108**, 16-34, https://doi.org/10.1111/j.1365-246X.1992.tb00836.x

Zhang, J. and Cunningham, D. 2012. Kilometer-scale refolded folds caused by strike-slip reversal and intraplate shortening in the Beishan region, China. *Tectonics*, **31**, https://doi.org/https://doi.org/10.1029/2011TC003050

Zhang, J., Cunningham, D. *et al.* 2021. Kinematic variability of late Cenozoic fault systems and contrasting mountain building processes in the Alxa block, western China. *Journal of Asian Earth Sciences*, **205**, 104597, https://doi.org/https://doi.org/10.1016/j.jseaes.2020.104597

Zhang, J., Zhang, B. *et al.* 2023. Late Cenozoic deformation characteristics and mechanism of the Beishan-Alxa region. *Earth Science Frontiers*, **30**, 334 [in Chinese with English abstract].

Zhang, P.-Z., Molnar, P. and Xu, X. 2007. Late Quaternary and present-day rates of slip along the Altyn Tagh Fault, northern margin of the Tibetan Plateau. *Tectonics*, **26**, https://doi.org/https://doi.org/10.1029/2006TC002014

Zhang, Z., Deng, Y., Teng, J., Wang, C.-Y., Gao, R., Chen, Y. and Fan, W. 2011. An overview of the crustal structure of the Tibetan Plateau after 35 years of deep seismic soundings. *Journal of Asian Earth Sciences*, **40**, 977-989, https://doi.org/10.1016/j.jseaes.2010.03.010

Zhang, Z., Xin, H. *et al.* 2020. The discovery of the Elegen ophiolite in Beishan orogenic belt, Inner Mongolia: Evidence for the east extension of the Hongshishan-Baiheshan ophiolite belt. *Geological Bulletin of China*, **39**, 1389-1403 [in Chinese with English abstract].

Zhao, G., Wu, Z., Liu, J., Zhang, L. and Zuo, J. 2019. The time space distribution characteristics and migration law of large earthquakes in the Indiam-Eurasian plate collision deformation area. *Journal of Geomechanics*, **25**, 324-340 [in Chinese with English abstract].

Zhao, G., Wang, Y., Huang, B., Dong, Y., Li, S., Zhang, G. and Yu, S. 2018. Geological reconstructions of the East Asian blocks: From the breakup of Rodinia to the assembly of Pangea. *Earth-Science Reviews*, **186**, 262-286, https://doi.org/https://doi.org/10.1016/j.earscirev.2018.10.003

Zhao, L., Li, Y. *et al.* 2024. Geochronology and geochemistry of early Paleozoic magmatism in the Qilian orogen: Constraints on closure of the Proto-Tethys Ocean. *Gondwana Research*, **126**, 223-242,

https://doi.org/10.5194/egusphere-2025-3096
Preprint. Discussion started: 10 July 2025


https://doi.org/https://doi.org/10.1016/j.gr.2023.10.006

Zheng, D., Wang, W. *et al.* 2017. Progressive northward growth of the northern Qilian Shan–Hexi Corridor (northeastern Tibet) during the Cenozoic. *Lithosphere*, **9**, 408-416, https://doi.org/10.1130/l587.1

Zheng, Y., Zhang, Q. *et al.* 1996. Great Jurassic thrust sheets in Beishan (North Mountains)—Gobi areas of China and southern Mongolia. *Journal of Structural Geology*, **18**, 1111-1126, https://doi.org/https://doi.org/10.1016/0191-8141(96)00038-7

Zong, K., Liu, Y., Zhang, Z., He, Z., Hu, Z., Guo, J. and Chen, K. 2013. The generation and evolution of Archean continental crust in the Dunhuang block, northeastern Tarim craton, northwestern China. *Precambrian Research*, **235**, 251-263, https://doi.org/https://doi.org/10.1016/j.precamres.2013.07.002

Zuo, G. and Liu, J. 1987. The evolution of tectonic of Early Paleozoic in North Qilian range, China. *Chinese Journal of Geology*, **22**, 14-24 [in Chinese with English abstract].

Zuo, G. and Li, S. 2011. Early Paleozoic tectonic framework and evolution in the northeast margin of Tarim Basin. *GEOLOGY IN CHINA*, **38**, 945-960 [in Chinese with English abstract].

Zuo, G., Zhang, S., He, G. and Zhang, Y. 1991. Plate tectonic characteristics during the early paleozoic in Beishan near the Sino-Mongolian border region, China. *Tectonophysics*, **188**, 385-392, https://doi.org/https://doi.org/10.1016/0040-1951(91)90466-6

Zuza, A.V., Cheng, X. and Yin, A. 2016. Testing models of Tibetan Plateau formation with Cenozoic shortening estimates across the Qilian Shan–Nan Shan thrust belt. *Geosphere*, **12**, 501-532, https://doi.org/10.1130/GES01254.1

Zuza, A.V., Wu, C., Wang, Z., Levy, D.A., Li, B., Xiong, X. and Chen, X. 2019. Underthrusting and duplexing beneath the northern Tibetan Plateau and the evolution of the Himalayan-Tibetan orogen. *Lithosphere*, **11**, 209-231, https://doi.org/10.1130/L1042.1

Zuza, A.V., Wu, C. *et al.* 2017. Tectonic evolution of the Qilian Shan: An early Paleozoic orogen reactivated in the Cenozoic. *GSA Bulletin*, **130**, 881-925, https://doi.org/10.1130/B31721.1

https://doi.org/10.5194/egusphere-2025-3096
Preprint. Discussion started: 10 July 2025


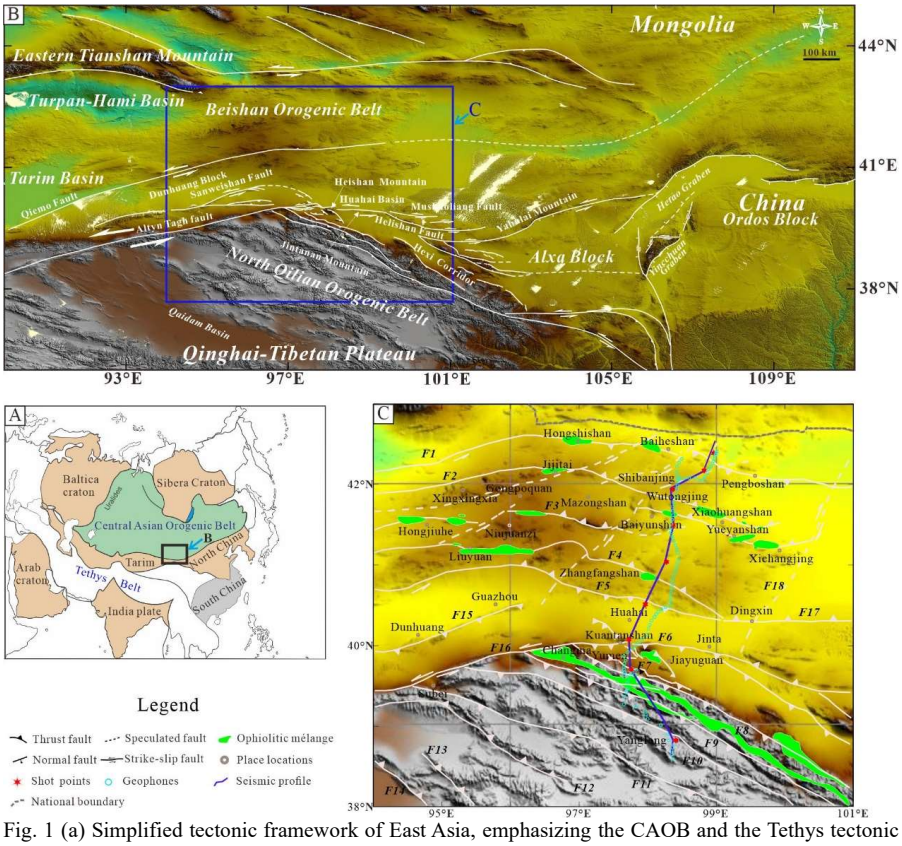


Fig. 1 (a) Simplified tectonic framework of East Asia, emphasizing the CAOB and the Tethys tectonic belt (modified after Xiao *et al.* 2017), and (b) distribution of main faults in NE Tibet and Beishan block (modified from Zhang *et al.* 2023), (c) location of the seismic profile, faults and ophiolite mélange zones. F0: North margin fault of the East Kunlun; F1: the Hongshishan-Baiyueshan-Pengboshan suture zone; F2: the Jijitai-Shibanjing-Xiaohuangshan fault; F3: the Hongliuhe-Baiyunshan-Yueyashan-Xichangjing suture zone; F4: the Liuyuan-Zhangfangshan suture zone; F5:the southern margin fault of the Beishan; F6: the Heishan-Jinta Nanshan; F7: the Yumen-Shuigoukou fault; F8: the northern margin fault of the North Qilian; F9: the North Qilian fault; F10: the northern margin fault of the Middle Qilian; F11: the southern margin fault of the Middle Qilian; F12: the Danghe Nanshan fault; F13: the southern margin fault of the South Qilian; F14: the northern margin fault of the Qaidam; F15: the Sanweishan fault; F16: the Altyn Tagh fault; F17: the northern margin fault of the Alxa; F18: the Ruoshui fault;

https://doi.org/10.5194/egusphere-2025-3096
Preprint. Discussion started: 10 July 2025


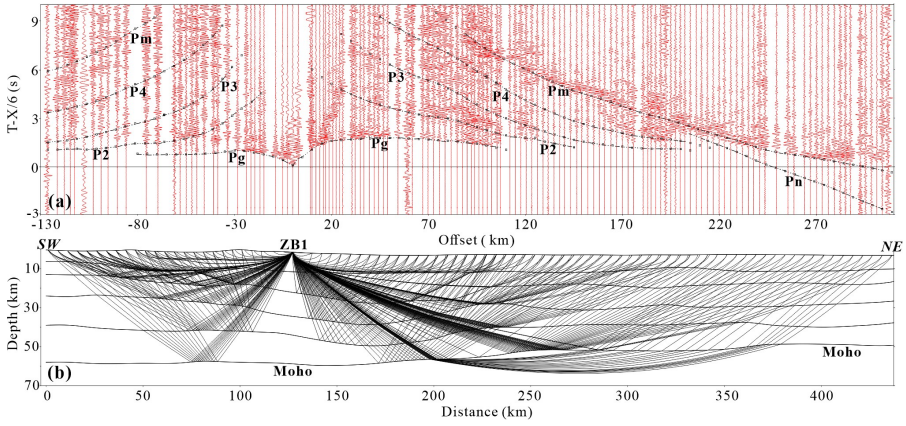


778 Fig. 2 P-wave record section (on a reduced time scale) corresponding to the shot point ZB1 and
779 identified seismic phases. The seismic phases are marked by dotted lines, and the squares mark the
780 location of calculated traveltime.

781

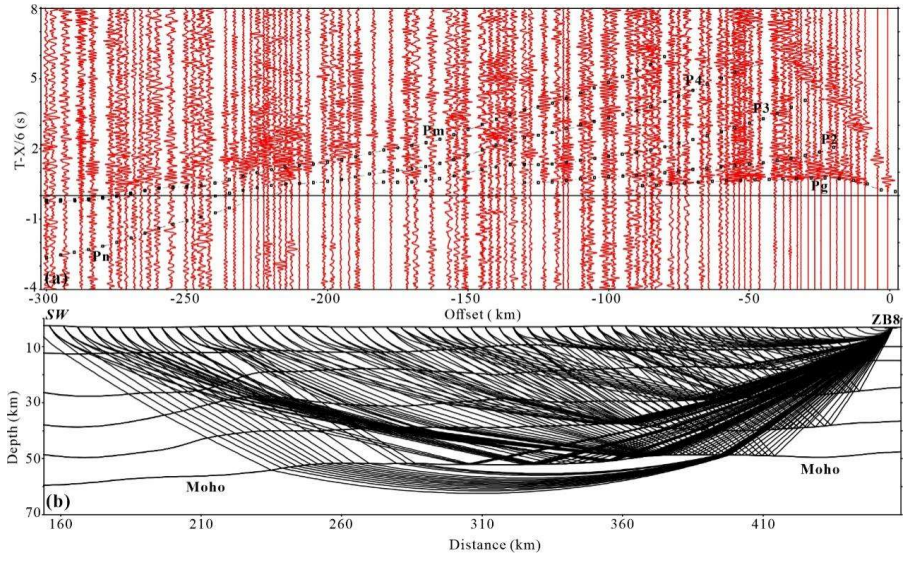


782

783 Fig. 3 P-wave record section (on a reduced time scale) corresponding to the shot point ZB8
784 and identified seismic phases. The seismic phases are marked by dotted lines, and the squares
785 indicate the location of calculated traveltime.
786

787

https://doi.org/10.5194/egusphere-2025-3096
Preprint. Discussion started: 10 July 2025


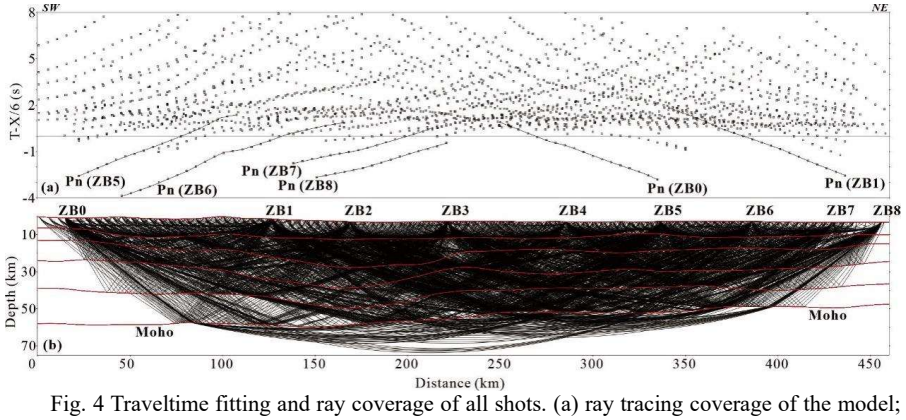


Fig. 4 Traveltime fitting and ray coverage of all shots. (a) ray tracing coverage of the model; (b) rays of all the phases for nine shots.

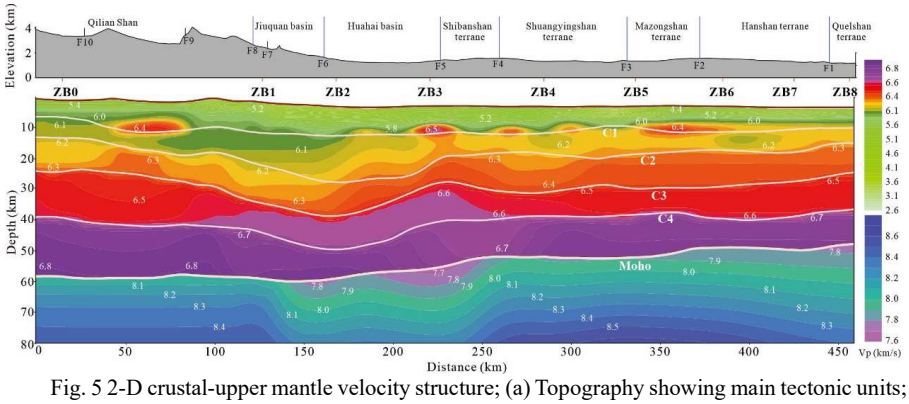


Fig. 5 2-D crustal-upper mantle velocity structure; (a) Topography showing main tectonic units; (b) crustal-upper mantle velocity structure. White solid lines denote the main interfaces.

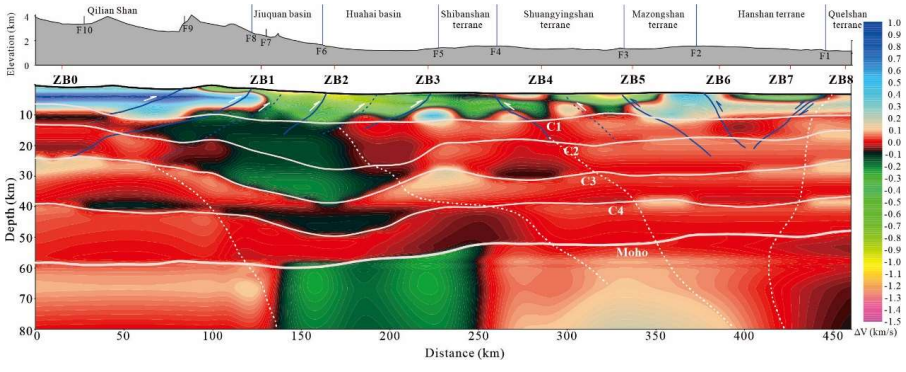


Fig. 6 2-D crustal- upper mantle velocity anomality structure; (a) Topography showing the main tectonic units; (b) crustal-upper mantle velocity anomality structure. White solid lines denote the main interfaces.

https://doi.org/10.5194/egusphere-2025-3096
Preprint. Discussion started: 10 July 2025


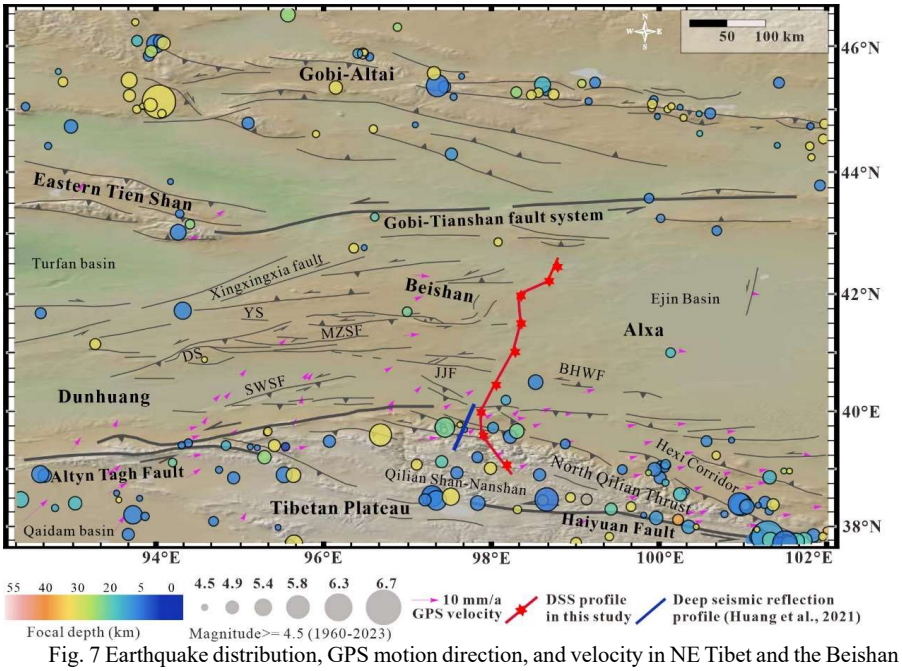


Fig. 7 Earthquake distribution, GPS motion direction, and velocity in NE Tibet and the Beishan block (modified from Yang et al., 2021). Purple arrows indicate GPS vectors relative to stable Siberia. BHWF: Beihewan Fault; JJF: Jiujing fault system; MZSF: Mazongshan fault system; SWSF: Sanweishan Fault; DS: Daquan Shan; YS: Yushi Shan.

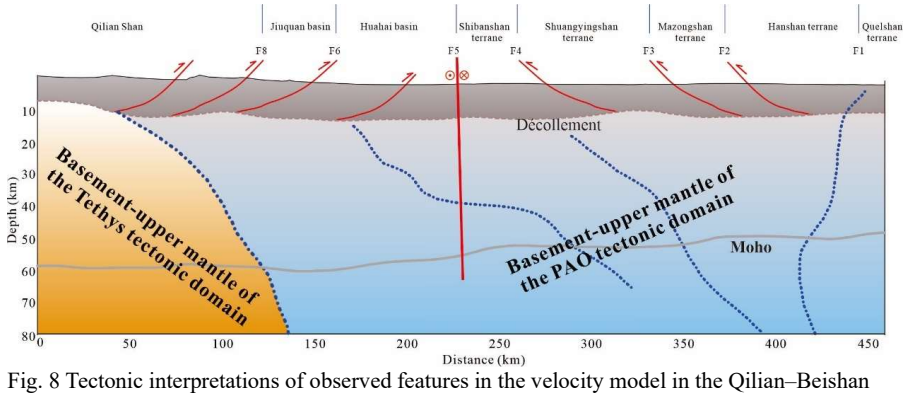


Fig. 8 Tectonic interpretations of observed features in the velocity model in the Qilian–Beishan area. Blue dotted lines represent the subduction direction of the fossil subduction slabs. Faults (F1-F8) align with Fig.1.

https://doi.org/10.5194/egusphere-2025-3096
Preprint. Discussion started: 10 July 2025


807 **Table 1 Explosion position of the deep seismic sounding profile**
808

| Shot No. | longitude(° E) | latitude(° N) | elevation(m) | TNT charge (kg) | Shot time (UTC+8) |
|---|---|---|---|---|---|
| ZB0 | 98.406 | 38.825 | 3387 | 2000 | 00:00:04.900 |
| ZB1 | 97.761 | 39.702 | 2466 | 2000 | 23:59:46.890 |
| ZB2 | 97.724 | 40.074 | 1447 | 2000 | 23:01:44.285 |
| ZB3 | 97.965 | 40.512 | 1334 | 1500 | 22:04:11.157 |
| ZB4 | 98.271 | 41.038 | 1302 | 1500 | 22:01:44.340 |
| ZB5 | 98.367 | 41.495 | 1341 | 2000 | 22:00:13.350 |
| ZB6 | 98.364 | 41.937 | 1520 | 3000 | 23:00:27.270 |
| ZB7 | 98.818 | 42.172 | 1243 | 2000 | 20:05:02.438 |
| ZB8 | 98.958 | 42.387 | 1154 | 3000 | 23:03:05.596 |

809

https://doi.org/10.5194/egusphere-2025-3096
Preprint. Discussion started: 10 July 2025


**Table 2 The RMS error of traveltime fitting for different seismic phases**

| Shot | Pg | | P2 | | P3 | | P4 | | Pm | | Pn | |
|---|---|---|---|---|---|---|---|---|---|---|---|---|
| | No. of picks | RMS time (s) | No. of picks | RMS time (s) | No. of picks | RMS time (s) | No. of picks | RMS time (s) | No. of picks | RMS time (s) | No. of picks | RMS time (s) |
| **ZB0** | 16 | 0.0251 | 26 | 0.0137 | 33 | 0.0169 | 37 | 0.0144 | 47 | 0.0159 | 17 | 0.0127 |
| **ZB1** | 58 | 0.021 | 58 | 0.02 | 57 | 0.0268 | 57 | 0.0207 | 75 | 0.0248 | 26 | 0.0265 |
| **ZB2** | 52 | 0.0309 | 46 | 0.032 | 46 | 0.0238 | 55 | 0.0244 | 51 | 0.0266 | 17 | 0.0275 |
| **ZB3** | 48 | 0.0157 | 60 | 0.0226 | 61 | 0.0144 | 59 | 0.0158 | 44 | 0.0123 | | |
| **ZB4** | 35 | 0.0274 | 39 | 0.0216 | 36 | 0.0218 | 39 | 0.0351 | 35 | 0.0206 | | |
| **ZB5** | 31 | 0.0118 | 29 | 0.0108 | 43 | 0.0191 | 34 | 0.0189 | 48 | 0.0225 | 13 | 0.0204 |
| **ZB6** | 33 | 0.0228 | 36 | 0.0155 | 37 | 0.0254 | 41 | 0.0204 | 61 | 0.0218 | 19 | 0.0256 |
| **ZB7** | 32 | 0.0246 | 29 | 0.019 | 31 | 0.0221 | 33 | 0.0197 | 48 | 0.018 | 21 | 0.0238 |
| **ZB8** | 28 | 0.0309 | 25 | 0.033 | 33 | 0.0233 | 55 | 0.0228 | 53 | 0.0272 | 12 | 0.0228 |
| **Mean RMS time (s)** | | **0.0234** | | **0.0209** | | **0.0215** | | **0.0214** | | **0.0211** | | **0.0227** |
| **Total picks** | **333** | | **348** | | **377** | | **410** | | **462** | | **125** | |